PHYSICAL REVIEW B **95**, 220201(R) (2017)

# Spontaneous natural optical activity in disordered media

F. A. Pinheiro,[1] V. A. Fedotov,[2] N. Papasimakis,[2] and N. I. Zheludev[2,3]

[1] *Instituto de Física, Universidade Federal do Rio de Janeiro, Rio de Janeiro-RJ 21941-972, Brazil*

[2] *Optoelectronics Research Centre and Centre for Photonic Metamaterials, University of Southampton, United Kingdom*

[3] *Centre for Disruptive Photonic Technologies, School of Physical and Mathematical Sciences and The Photonics Institute, Nanyang Technological University, Singapore*

(Received 26 October 2016; revised manuscript received 30 May 2017; published 20 June 2017)

We theoretically demonstrate natural optical activity in disordered ensembles of nonchiral plasmonic resonators. We show that the statistical distributions of rotatory power and spatial dichroism are strongly dependent on the scattering mean free path in diffusive random media. This result is explained in terms of the intrinsic geometric chirality of disordered media, as they lack mirror symmetry. We argue that chirality and natural optical activity of disordered systems can be quantified by the standard deviation of both rotatory power and spatial dichroism. Our results are based on microscopic electromagnetic wave transport theory coupled to vectorial Green's matrix method for pointlike scatterers and are independently confirmed by full-wave simulations.

DOI: 10.1103/PhysRevB.95.220201

The concept of chirality, introduced by Lord Kelvin to designate any geometrical object that lacks mirror symmetry, pervades the natural world. The DNA double-helix structure and the related long-standing enigma of the origin of homochirality of life are just some examples of this fundamental concept in science [1]. Since the pioneer work by Pasteur on the resolution of tartaric acid, the development of efficient synthesis processes of naturally occurring chiral molecules is of utmost importance [1]. In addition to natural chiral systems, designing artificial chiral structures constitutes an intense research activity recently [2]. Chiral metamaterials are striking examples of artificial media without mirror symmetry [3]; they have been applied to generate novel optical properties such as negative index media [4,5], broadband circular polarizers [6], and enantioselective photochemistry [7]. Another possibility of artificially generating chiral systems is to assembly achiral plasmonic nanoparticles in standard chiral geometries, such as helices [8–15]. Remarkably, natural optical activity (NOA) in these systems can be considerably larger than in molecular ones. Also, the conditions for observing NOA have been recently revisited [16–18].

Despite all efforts to understand the optical properties of naturally occurring chiral media and to design artificial ones, there is an important yet overlooked class of chiral systems: disordered structures. Such systems have neither center nor plane of symmetry, so that they should exhibit NOA as any other chiral medium. Interestingly, there is some previous experimental evidence of NOA in random media, but this effect has never been attributed to the presence of disorder [19–22]; instead, alternative explanations, such as surface contamination by unwanted chiral substances, have been put forward [20,21].

Here, we theoretically demonstrate NOA due to intrinsic geometric chirality in disordered, diffusive scattering systems composed of pointlike scatterers (see Fig. 1). Using microscopic electromagnetic wave transport theory, we demonstrate that the standard deviation of rotatory power and spatial dichroism are strongly dependent on the scattering mean free path. We show that NOA in disordered ensembles can be more than an order of magnitude higher than in the archetypical helical configurations [14]. By unveiling that random systems are chiral, and how this fundamental property shows up in a physical observable (NOA), our findings may not only theoretically explain previous experimental results [20–22] but also provide a new systematic way to optically characterize disordered media. Indeed, our results demonstrate how one can probe chirality of random media, a ubiquitous class of materials in nature that includes a broad range of physical systems, such as clouds of atomic scatterers, small dielectric scatterers, disordered plasmonic resonators, and metamaterials.

To derive the expression for NOA in disordered media we use the well established microscopic theory of vector wave diffusion [23]. The tensor $\mathbf{d_p}$ represents the specific intensity of the diffuse radiation in the direction $\mathbf{p}$ [24]:

$$\mathbf{d_p}(\mathbf{q}) = i[\mathbf{G_p} - \mathbf{G_p^*}] - i\mathbf{G_p} \cdot \Gamma_\mathbf{p}(\mathbf{q}) \cdot \mathbf{G_p^*}, \qquad (1)$$

with $\mathbf{G_p} = [\omega^2 - p^2 + \mathbf{pp} - \Sigma_\mathbf{p}]^{-1}$ the Dyson Green's tensor. For a low density $n$ of the scatterers the mass-operator $\Sigma_\mathbf{p}$ is related to the T matrix of one independent scatterer according to $\Sigma_\mathbf{p} = n\mathbf{t_{pp}}$ [23,25]. In Eq. (1) $\Gamma_\mathbf{p}$ describes the angular dependence of the diffuse energy flow; it obeys the integral equation [24,26,27]

$$\Gamma_\mathbf{p}(\mathbf{q}) = \mathbf{L_p}(\mathbf{q}) + \sum_{\mathbf{p}'} \Gamma_{\mathbf{p}'}(\mathbf{q}) \cdot \mathbf{G}_{\mathbf{p}'} \otimes \mathbf{G}^*_{\mathbf{p}'} \cdot \mathbf{U}_{\mathbf{pp}'}, \qquad (2)$$

where $\mathbf{L_p}(\mathbf{q})$ is the current tensor and $\mathbf{U}_{\mathbf{pp}'}$ the irreducible vertex [23].

In isotropic chiral media, the tensor $\Gamma_\mathbf{p}$ (neglecting longitudinal terms) takes the form [28]:

$$\Gamma_\mathbf{p}(\mathbf{q}) = \gamma_0(\mathbf{p}\cdot\mathbf{q})\Delta_\mathbf{p} + \gamma_C(\mathbf{p}\cdot\mathbf{q})\Phi_{\hat{\mathbf{p}}}, \qquad (3)$$

where $\Delta_\mathbf{p}$ is the projector upon the space of transverse polarization (normal to $\mathbf{p}$), and $\Phi$ is the antisymmetric Hermitian tensor $\Phi_{ij} = i\epsilon_{ijk}\hat{p}_k$ ($\epsilon_{ijk}$ being the Levi-Civita tensor). In chiral media $\Gamma_\mathbf{p}(\mathbf{q})$ obeys the symmetry relation $\Gamma_\mathbf{p}(\mathbf{q}) = -\Gamma_{-\mathbf{p}}(\mathbf{q}) = \Gamma_{-\mathbf{p}}(-\mathbf{q})$.

Our objective is to solve Eq. (2) and to explicitly obtain the coefficients $\gamma_0$, $\gamma_C$ in Eq. (3) and an expression for NOA. To this end, let us separate the mass operator $\Sigma_\mathbf{p}$ in a symmetric

 

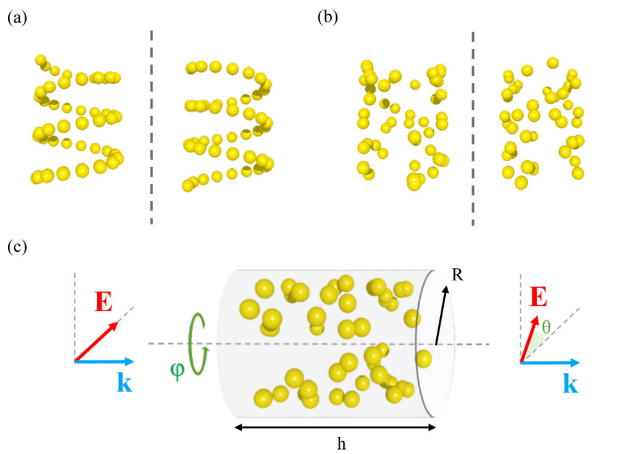


FIG. 1. Examples of chiral ensembles with their respective mirror images: dipole scatterers arranged in a helix (a) and in a random configuration (b). (c) Schematic representation of polarization rotation in a disordered medium, where $\theta$ corresponds to polarization rotations.

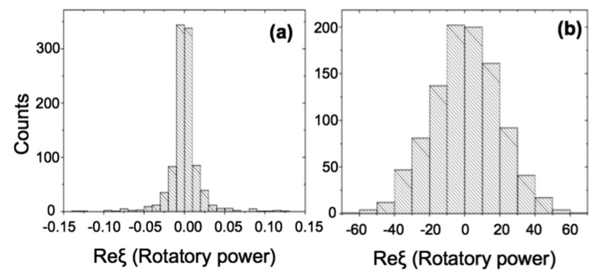


FIG. 2. Histogram of Re$\xi$ that gives the rotatory power in disordered medium for (a) 10 and (b) 700 pointlike scatterers randomly distributed inside a cylinder of fixed volume (height $h/\lambda = 10$ and radius $R/\lambda \simeq 5$). The values of Re$\xi$ have been normalized by the ones corresponding to 100 scatterers distributed along a helix (radius $5\lambda$, pitch $2\lambda$, height $10\lambda$).

(S) and an antisymmetric (A) part:

$$\Delta\Sigma_{\mathbf{p}} \equiv -\left(\mathrm{Im}\Sigma^S_{\mathbf{p}} + \mathrm{Im}\Sigma^A_{\mathbf{p}}\right) = -\mathrm{Im}\Sigma_{\mathbf{p}}(\mathbf{U} + \xi\Phi_{\hat{\mathbf{p}}}). \tag{4}$$

Equation (5) defines the pseudoscalar $\xi$, whose real and imaginary parts determines the rotatory power and the spatial dichroism of the effective medium, respectively. Inserting Eq. (3) into Eq. (2) and performing the operations $\int \frac{d\hat{\mathbf{p}}}{4\pi}\mathrm{Tr}\Delta_{\mathbf{p}}$ and $\int \frac{d\hat{\mathbf{p}}}{4\pi}\mathrm{Tr}\Phi_{\mathbf{p}}$ results in the two following coupled equations for $\gamma_0$ and $\gamma_C$:

$$\gamma_0 = 2 + g\left(\frac{\gamma_0 + \xi\gamma_C}{1+\xi^2}\right) + g_C\left(\frac{\gamma_C - \xi\gamma_0}{1+\xi^2}\right), \tag{5}$$

$$\gamma_C = -g_C\left(\frac{\gamma_0 + \xi\gamma_C}{1+\xi^2}\right) - g_{CC}\left(\frac{\gamma_C - \xi\gamma_0}{1+\xi^2}\right). \tag{6}$$

It can be shown that $g$, $g_C$, $g_{CC}$, and $\xi$ can be explicitly written in terms of the scattering total T matrix of an ensemble of $N$ point dipoles [28], which describes multiple scattering from the direction $\mathbf{p}$ to $\mathbf{p}'$

$$\mathbf{T}_{\mathbf{pp}'} = \sum_{NN'} \mathbf{S}^{NN'} \exp(-i\mathbf{p}\cdot\mathbf{r}_N + i\mathbf{p}'\cdot\mathbf{r}_{N'}), \tag{7}$$

with $\mathbf{S}^{NN'}$ the matrix describing scattering of light from particle $N$ to $N'$ that is obtained by diagonalization [29]. As a result, multiple scattering is treated exactly, i.e., all scattering orders are included; the only approximation within this model is at the level of single scattering, as scatterers are treated as point dipoles. In terms of $\mathbf{S}^{NN'}$, $\xi$ reads [28]

$$\xi = \frac{1}{2}\sum_{NN'} \mathrm{Tr}\{(\mathbf{S}^{NN'} \cdot \epsilon \cdot \hat{\mathbf{r}}_{NN'}) j_1(kr_{NN'})\}, \tag{8}$$

where $j_1(x)$ is the spherical Bessel function of the first kind, and $\mathbf{r}_{NN'}$ is the relative position between scatterers $N$ and $N'$. We have numerically verified that $\xi$ is indeed a pseudoscalar and that it vanishes for $N < 4$, reflecting the fact that a chiral system must be composed of at least four particles.

In Fig. 2 the distributions of Re$\xi$, which gives the optical rotatory power, is calculated using Eq. (8) for 1000 different disorder realizations and two different particle densities; the scatterers are randomly distributed inside a cylinder of fixed volume. In Fig. 2(a) Re$\xi$ is calculated for $N = 10$ resonant scatterers, which corresponds to $k\ell \approx 1000$ [with $k$ the wave number and $\ell = 1/(n\sigma)$ the mean free path, where $\sigma = 3\lambda^2/2\pi$ is the cross section of a resonant point scatterer]. We have considered resonant scatterers to facilitate multiple light scattering, as the cross section of point dipoles is maximal at resonance [27]. In Fig. 2(b) Re$\xi$ is calculated for $N = 700$ scatterers, in which case multiple light scattering is stronger ($k\ell \approx 15$). For both densities light transport in the random medium is diffusive. Re$\xi$ have been normalized by the ones corresponding to 100 scatterers distributed along a helix inside a cylinder of equal volume [see Fig. 1(a)]. Figure 2(b) reveals that for a given configuration of random scatterers the value of rotatory power can be up to 60 times larger than for a system with the same density, where the particles are distributed along a helix, which is the hallmark of a chiral system. Figure 2 also shows that $\langle\xi\rangle = 0$, which can be explained by the fact that for a large number of disorder realizations the mirror image of any configuration is equally probable. However, Fig. 2 demonstrates that the standard deviation of the distribution of Re$\xi$ is strongly dependent on $\ell$, which is a measure of how strong light scattering is inside the medium. We have verified that the standard deviation of Im$\xi$ exhibits a similar dependence on $\ell$.

Figure 3 shows the real (Re$\sigma_\xi$) and imaginary (Im$\sigma_\xi$) parts of the standard deviation of $\xi$ for 1000 disorder realizations as a function of $k\ell$ for a diffusive system ($10 \lesssim k\ell \lesssim 3000$) composed of resonant pointlike scatterers randomly distributed inside a cylinder of fixed volume. For these values of $k\ell$ dipole-dipole interactions are expected to be negligible [30]. The results are normalized by the value of $\xi$ for a system composed of 100 scatterers distributed along a helix contained in a cylinder of equal volume. This allows us to obtain the order-of-magnitude of NOA of a disordered medium, as NOA for nanoparticles oriented along a helix has been calculated in Ref. [14]. Figure 3 reveals that $\sigma_\xi$ monotonically increases as $k\ell$ decreases, showing that the magnitude of NOA increases as the density of scatterers increases. More importantly, for $k\ell \lesssim 20$ $\sigma_\xi$ can be approximately 15 times

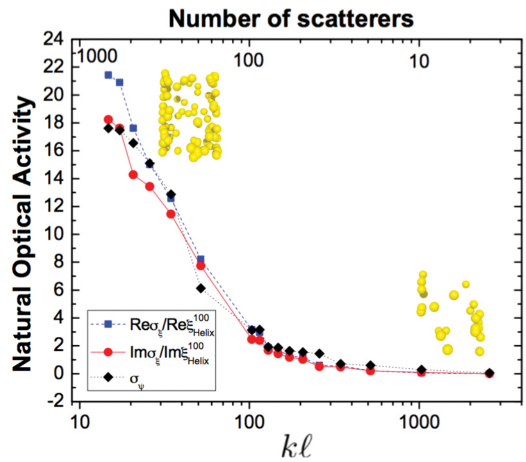


FIG. 3. The standard deviation of the distributions of $\xi$, $\sigma_\xi$, for 1000 configurations of randomly distributed identical pointlike scatterers inside a inside a cylinder of fixed volume (height $h/\lambda = 10$ and radius $R/\lambda \simeq 5$) as a function of $k\ell$. The top horizontal axis shows the corresponding number of particles inside the cylinder. Re$\xi$ and Im$\xi$ have been normalized by $\mathrm{Re}\xi^{100}_{\mathrm{Helix}}$ and $\mathrm{Im}\xi^{100}_{\mathrm{Helix}}$, which correspond to rotatory power and spatial dichroism of 100 pointlike dipoles distributed along a helix (radius $5\lambda$, pitch $2\lambda$, height $10\lambda$) inside a cylinder of the same volume. Also shown is the standard deviation $\sigma_\psi$ of the distributions of chiral geometrical parameter $\psi$, defined in Ref. [31], of the corresponding 1000 random configurations. The insets show characteristic random configurations for high and low particle densities.

larger than the case of a helix. Both Re$\sigma_\xi$ and Im$\sigma_\xi$ are small for ballistic and weakly scattering systems, for which $k\ell \gg 1$. This demonstrates that multiple light scattering is necessary in order to produce significant values of NOA. We have verified that at least four scattering events are required to generate a nonvanishing value of $\xi$, so that light can "probe" the chiral configuration associated to random scatterers.

To further investigate the interplay between the chirality associated with the random configuration of particles and NOA, in Fig. 3 we also calculate the geometrical chiral index $\psi$ defined in [31]. $\psi$, which only depends on the scatterers positions, is a pseudoscalar invariant under rotations that vanishes for achiral configurations [31]. The choice of chiral index is not unique and other chiral measures do exist [32]. The chiral index $\psi$ has been chosen here by its simplicity and, more importantly, because it has been shown to be related to physical observables, such as the magnetochiral scattering cross section [33], the electronic current in chiral carbon nanotubes [34], and the pitch of a cholesteric liquid crystal [31]. For a random ensemble of scatterers the average value of $\psi$ over many disorder realizations is zero since the mirror image of any configuration is equally probable. However, the standard deviation $\sigma_\psi$ is strongly dependent on the particle density. This can be seen in Fig. 3, where $\sigma_\psi$ is calculated for 1000 disorder realizations. Remarkably, Fig. 3 shows that $\sigma_\psi$ is proportional to $\sigma_\xi$, confirming that the calculated optical activity is indeed related to the intrinsic chirality of disordered systems. Together with previous experimental evidence of NOA in disordered systems in the absence of any chiral substance [20–22], these results strongly suggest that large

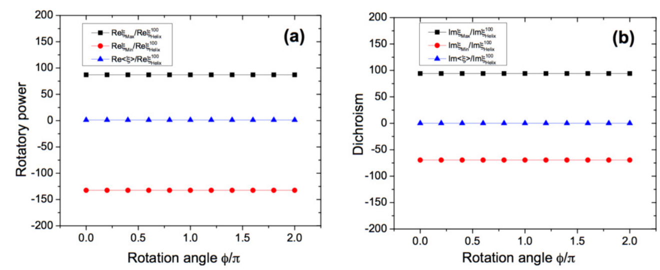


FIG. 4. (a) The maximal (black squares), minimum (red circles), and average (blue triangles) values of Re$\xi$, from 1000 fixed, distinct random configurations of 100 dipoles inside a cylinder of the same volume as a function of the rotation angle $\phi$ around the cylinder main axis [see Fig. 1(c)]. Figure 4(b) shows the analogous for Im$\xi$. Re$\xi$ and Im$\xi$ are normalized by $\mathrm{Re}\xi^{100}_{Helix}$ and $\mathrm{Im}\xi^{100}_{Helix}$ that correspond to the values of $\xi$ for 100 scatterers distributed along a helix (radius $5\lambda$, pitch $2\lambda$, height $10\lambda$) inside a cylinder of the same volume.

optical activity should be observed in a disordered medium. As a possible application, Fig. 3 suggests that one could determine the particle density in solution by measuring NOA.

To investigate whether the calculated NOA is related to the anisotropy of the disordered medium, we have calculated Re$\xi$ and Im$\xi$ for 1000 random configurations of scatterers inside a cylinder with the dimensions of Fig. 2 under continuous rotation by an angle $\phi$ around the cylinder axis [Fig. 1(c)]. We have numerically verified that for all realizations $\xi$ does not depend on $\phi$ as shown in Fig. 4, where we present the maximal, minimum, and average values of $\xi$ as a function of $\phi$ for all realizations. Hence anisotropy contributions to the reported results can be ruled out. Indeed, polarization change due to anisotropy does not require multiple light scattering. On the contrary, here optical activity is related to the intrinsic chirality of random media, which light can only probe when multiple scattering occurs (or, more precisely, when at least four scattering events occur) (Fig. 3).

All results presented so far are general and can be applied to a broad range of physical systems, as the point-dipole model [27], on which our results are grounded, can describe successfully multiple light scattering in various random media, such as clouds of atomic gases [35,36], ensembles of small dielectric scatterers [29], and disordered plasmonic resonators and random metamaterials [37]. In the following we focus on plasmonic systems and consider random and helical configurations of achiral Au nanoparticles. In Fig. 5, we show differential absorption ($\Delta A$) for circularly polarized light as a function of wavelength for random and helical ensembles of 25 nanoparticles, calculated by the finite element method (see Supplemental Material [38] for details). In both cases, the density is $\simeq$4 nanoparticles/$\lambda^3$, so that light transport is diffusive, and hence corrections of high order multipoles can be neglected. The helical configuration exhibits strong differential absorption in the vicinity of the plasmonic resonance ($\simeq$525 nm). In the case of random ensembles, the average over 310 realizations is close to zero, as predicted by the previous microscopic analysis. However, the standard deviation ($\sigma_{\Delta A}$) exceeds the $\Delta A$ of the helical configuration by a factor of 2 at resonance. These results are in qualitative agreement with the point-dipole model predictions, and demonstrate

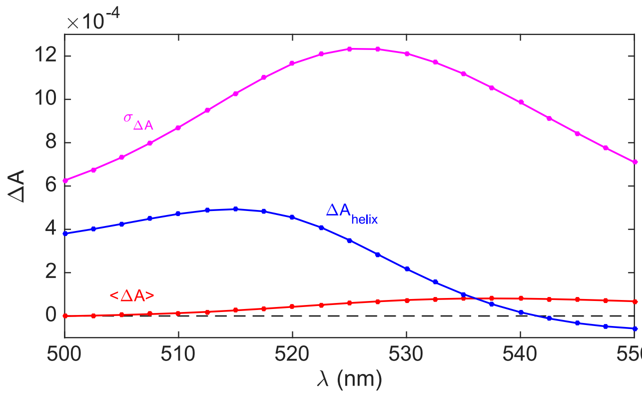


FIG. 5. Differential absorption ($\Delta A$) spectra of random and helical Au nanoparticle (25 nm radius) configurations under illumination with left- and right-circularly polarized light. Blue line represents the $\Delta A$ of a helical arrangement with radius = 467 nm & pitch = 660 nm., while the red line shows Tte average, $\langle \Delta A \rangle$, over 310 realizations of random configurations. Magenta line represents the standard deviation $\sigma_{\Delta A}$ of $\Delta A$. All spectra are obtained by finite element modeling (see Supplemental Material [38] for details).

unambiguously that polarization effects in such systems can be much stronger than in a typical chiral medium (helix).

We note that the optical activity of disordered media could be observed in various physical systems, such as cold atomic clouds or ensembles of plasmonic nanoparticles. In the latter example, one can perform polarimetry measurements in colloidal suspensions of gold nanoparticles at the plasmonic resonance wavelength. Concentrations similar to those considered here are commercially available. Even for a very small number of particles ($N = 25$), the predicted difference in extinction under illumination with left- and right- circularly polarized light (see Supplemental Material [38]) can be experimentally observed with existing techniques [39]. Different realizations can be obtained by different measurements in time, since the nanoparticle configuration changes slowly due to the movement of the nanoparticles. Similar experiments can be performed in spin coated nanoparticle films, or even by structuring thin metallic films, which allows to accurately control the density and positioning of the scatterers.

In conclusion, we have investigated NOA of diffusive disordered systems composed of nonchiral scatterers. Using microscopic electromagnetic wave transport theory, we have demonstrated that the distributions of the rotatory power and spatial dichroism in such systems is strongly dependent on the scattering mean free path, a result that is corroborated by full-wave electromagnetic calculations. We show that the standard deviation of a purely geometrical chiral parameter is proportional to the standard deviation of NOA in random media. This finding indicates that the latter is the appropriate quantity to probe NOA in disordered media, which is intrinsically related to the fact that random systems lack mirror symmetry.

We thank B. A. van Tiggelen, L. Dal Negro, and O. Buchnev for fruitful discussions. We acknowledge the support of CAPES (Estagio Sênior BEX 1497/14-6), CNPq (303286/2013-0), the Royal Society (Newton Advanced Fellowship NA150208), and the UK's Engineering and Physical Sciences Research Council (EP/M008797/1).

[1] G. H. Wagniére, *On Chirality and the Universal Asymmetry: Reflections on Image and Mirror Image* (Wiley-VCH, Zurich, 2007).
[2] A. Guerrero-Martinez, J. L. Alonso-Gómez, B. Auguié, M. M. Cid, and L. M. Liz-Marzána, Nanotoday **6**, 381 (2011).
[3] A. V. Rogacheva, V. A. Fedotov, A. S. Schwanecke, and N. I. Zheludev, Phys. Rev. Lett. **97**, 177401 (2006).
[4] B. Pendry, Science **306**, 1353 (2004).
[5] E. Plum, J. Zhou, J. Dong, V. A. Fedotov, T. Koschny, C. M. Soukoulis, and N. I. Zheludev, Phys. Rev. B **79**, 035407 (2009).
[6] J. K. Gansel, M. Thiel, M. S. Rill, M. Decker, K. Bade, V. Saile, G. von Freymann, S. Linden, and M. Wegener, Science **325**, 1513 (2009).
[7] Y. Tang and A. Cohen, Science **332**, 333 (2011).
[8] A. Papakostas, A. Potts, D. M. Bagnall, S. L. Prosvirnin, H. J. Coles, and N. I. Zheludev, Phys. Rev. Lett. **90**, 107404 (2003).
[9] S. Boruhovich, S. L. Prosvirnin, A. S. Schwanecke, and N. I. Zheludev, Proc. Eur. Microw. Assoc. **2**, 89 (2006).
[10] V. K. Valev, J. J. Baumberg, C. Sibilia, and T. Verbiest, Adv. Mater. **25**, 2517 (2013).
[11] A. Kuzyk, R. Schreiber, Z. Fan, G. Pardatscher, E.-M. Roller, A. Högele, F. C. Simmel, A. O. Govorov, and T. Liedl, Nature (London) **483**, 311 (2012).
[12] X. Shen, A. Asenjo-Garcia, Q. Liu, Q. Jiang, F. J. García de Abajo, N. Liu, and B. Ding, Nano Lett. **13**, 2128 (2013).
[13] M. Hentschel, M. Schäferling, T. Weiss, N. Liu, and H. Giessen, Nano Lett. **12**, 2542 (2012).
[14] Z. Fan and A. O. Govorov, Nano Lett. **10**, 2580 (2010).
[15] V. E. Ferry, J. M. Smith, and A. P. Alivisatos, ACS Photon. **1**, 1189 (2014).
[16] I. Fernandez-Corbaton, X. Vidal, N. Tischler, and G. Molina-Terriza, J. Chem. Phys. **138**, 214311 (2013).
[17] N. Tischler, I. Fernandez-Corbaton, X. Zambrana-Puyalto, A. Minovich, X. Vidal, M. L. Juan, and G. Molina-Terriza, Light: Sci. Applic. **3**, e183 (2014).
[18] I. Fernandez-Corbaton, M. Fruhnert, and C. Rockstuhl, ACS Photon. **2**, 376 (2015).
[19] X. Guo, M. F. G. Wood, and I. Alex Vitkin, Appl. Opt. **46**, 4491 (2007).
[20] K. C. Hadley and I. A. Vitkin, J. Biomed. Opt. **7**, 291 (2002).
[21] M. E Silverman, W. Strange, J. Badoz, and I. A. Vitkin, Opt. Commun. **132**, 410 (1996).
[22] V. P. Drachev, W. D. Bragg, V. A. Podolskiy, V. P. Safonov, W.-T. Kim, Z. C. Ying, R. L. Armstrong, and V. M. Shalaev, J. Opt. Soc. Am. B **18**, 1896 (2001).
[23] P. Sheng, *Wave Scattering, Localization and Mesoscopic Phenomena* (Academic Press, San Diego, 1995).
[24] G. D. Mahan, *Many-Particle Physics* (Plenum, New York, 1981).
[25] For point scatterers, the T matrix is equivalent to that of a two-level system exhibiting one resonant (electric dipole)

transition : $\mathbf{t}(\omega) = [-4\pi\Gamma\omega^2/(\omega_0^2 - \omega^2 - 2i\Gamma\omega^3/3c_0)]\mathbf{U}$, with $\omega_0$ being the resonance frequency, $\Gamma$ the resonance linewidth, and $\mathbf{U}$ the unit matrix [26,27]. The dynamic polarizability of the point scatterer relates to its T matrix according to $\boldsymbol{\alpha}(\omega) = -\mathbf{t}(\omega)/(\omega/c_0)^2$ [26,27].

[26] A. Lagendijk and B. A. van Tiggelen, Phys. Rep. **270**, 143 (1996).

[27] P. de Vries, D. V. van Coevorden, and A. Lagendijk, Rev. Mod. Phys. **70**, 447 (1998).

[28] F. A. Pinheiro and B. A. van Tiggelen, J. Opt. Soc. Am. A **20**, 99 (2003).

[29] F. A. Pinheiro, M. Rusek, A. Orlowski, and B. A. van Tiggelen, Phys. Rev. E **69**, 026605 (2004); F. A. Pinheiro, Phys. Rev. A **78**, 023812 (2008); M. Rusek, J. Mostowski, and A. Orlowski, *ibid.* **61**, 022704 (2000); A. Goetschy and S. E. Skipetrov, Phys. Rev. E **84**, 011150 (2011).

[30] S. E. Skipetrov and I. M. Sokolov, Phys. Rev. Lett. **112**, 023905 (2014).

[31] A. B. Harris, R. D. Kamien, and T. C. Lubensky, Rev. Mod. Phys. **71**, 1745 (1999).

[32] A. Potts, D. M. Bagnall, and N. I. Zheludev, J. Opt. A **6**, 193 (2004); G. Gilat, J. Phys. A **22**, L545 (1989); M. A. Osipov, B. T. Pickup, and D. A. Dunmur, Mol. Phys. **84**, 1193 (1995); M. P. Neal, M. Solymosi, M. R. Wilson, and D. J. Earl, J. Chem. Phys. **119**, 3567 (2003).

[33] F. A. Pinheiro and B. A. van Tiggelen, Phys. Rev. E **66**, 016607 (2002).

[34] F. A. Pinheiro, S. J. S. da Silva, E. R. Granhen, and J. Del Nero, Phys. Rev. B **81**, 115456 (2010).

[35] L. Bellando, A. Gero, E. Akkermans, and R. Kaiser, Phys. Rev. A **90**, 063822 (2014).

[36] S. E. Skipetrov and I. M. Sokolov, Phys. Rev. Lett. **114**, 053902 (2015).

[37] T. S. Kao, S. D. Jenkins, J. Ruostekoski, and N. I. Zheludev, Phys. Rev. Lett. **106**, 085501 (2011).

[38] See Supplemental Material at http://link.aps.org/supplemental/10.1103/PhysRevB.95.220201 for full details of the finite element calculations discussed in the main text.

[39] L. M. Payne, W. Langbein, and P. Borri, Appl. Phys. Lett. **102**, 131107 (2013).